Generalized Eulerian-Lagrangian description of Navier-Stokes dynamics

Carlos Cartes, Miguel D. Bustamante,[a] and Marc E. Brachet
Laboratoire de Physique Statistique de l'Ecole Normale Supérieure, associé au CNRS et aux Universités Paris VI et VII, 24 Rue Lhomond, 75231 Paris, France

(Received 18 December 2006; accepted 4 May 2007; published online 11 July 2007)

Generalized equations of motion for the Weber-Clebsch potentials that reproduce Navier-Stokes dynamics are derived. These depend on a new parameter, with the dimension of time, and reduce to the Ohkitani and Constantin equations in the singular special case where the new parameter vanishes. Let us recall that Ohkitani and Constantin found that the diffusive Lagrangian map became noninvertible under time evolution and required resetting for its calculation. They proposed that high frequency of resetting was a diagnostic for vortex reconnection. Direct numerical simulations are performed. The Navier-Stokes dynamics is well reproduced at small enough Reynolds number without resetting. Computation at higher Reynolds numbers is achieved by performing resettings. The interval between successive resettings is found to abruptly increase when the new parameter is varied from 0 to a value much smaller than the resetting interval. © *2007 American Institute of Physics*. [DOI: 10.1063/1.2748447]

I. INTRODUCTION

The classical[1] Eulerian-Lagrangian formulation of the (inviscid) Euler dynamics in terms of advected Weber-Clebsch potentials was recently extended to describe the (viscous) Navier-Stokes dynamics by Constantin.[2] Numerical studies of this Eulerian-Lagrangian formulation of the Navier-Stokes equations were then performed by Ohkitani and Constantin (OC).[3] They found that the diffusive Lagrangian map becomes noninvertible under time evolution and requires resetting for its calculation. They argued that this sets a time scale and its frequent resetting corresponds to vortex reconnection. The aim of the present paper is to complement these results. Our approach is based on a new generalized set of equations of motion for the Weber-Clebsch potentials. Our main conclusion is that the OC formulation is a special singular case of the new generalized formulation. Here follows a summary of our principal results.

We first derive the generalized equations of motion that turn out to depend on a new parameter τ (with the dimension of time). They are shown to reduce to the OC equations in the *singular* limit $\tau \to 0$. We then perform direct numerical simulations (DNS) of the viscous Taylor-Green (TG) vortex.[4] When $\tau \neq 0$, for small enough Reynolds numbers, the Navier-Stokes dynamics is well reproduced *without* resetting. Performing resettings allows computation at much higher Reynolds numbers, with errors that rapidly decay following each resetting. The interval Δt between successive resettings is finally found to sharply increase when τ is varied from 0 to a value much smaller than Δt.

II. THEORETICAL SETTING

In this section, we first derive a (generally underdetermined) linear system that, when obeyed by the convective derivative of the Weber-Clebsch potentials, implies that the velocity field follows the Navier-Stokes equations. Using the notion of Moore-Penrose[5–7] pseudoinverse, the linear system is supplemented by a requirement of minimum norm, which depends on a new parameter τ. The Moore-Penrose solution yields our new generalized equations of motion, which are finally shown to reduce to the OC equations of motion in the singular limit $\tau \to 0$.

A. Weber-Clebsch representation of acceleration

Our starting point will be the classical[1] Weber-Clebsch representation of the velocity field,

$$\mathbf{u} = \sum_{i=1}^{q} \lambda^i \nabla \mu^i - \nabla \phi, \tag{1}$$

where each of the q pairs of Weber-Clebsch potentials (λ^i, μ^i) is a scalar function of (d-dimensional) space and time, with coordinates $(x^1, \ldots, x^d, t)$.

Performing a variation on the Clebsch representation (1) yields the relation

$$\delta \mathbf{u} = \sum_{i=1}^{q} (\delta \lambda^i \nabla \mu^i - \delta \mu^i \nabla \lambda^i) - \nabla \left(\delta \phi - \sum_{i=1}^{q} \delta \mu^i \lambda^i \right), \tag{2}$$

where the symbol δ stands for any (spatial or temporal) partial derivative.

Defining the convective derivative

$$\frac{D}{Dt} \equiv \frac{\partial}{\partial t} + (\mathbf{u} \cdot \nabla), \tag{3}$$

and taking into account the identity $[\nabla, D/Dt] \equiv (\nabla \mathbf{u}) \cdot \nabla$, it is straightforward to derive from (2) the following explicit expression for the local acceleration:

[a]Present address: Mathematics Institute, University of Warwick, Coventry CV4 7AL, United Kingdom.

$$\frac{D\mathbf{u}}{Dt} = \sum_{i=1}^{q} \left(\frac{D\lambda^i}{Dt} \nabla \mu^i - \frac{D\mu^i}{Dt} \nabla \lambda^i \right) - \nabla \left(\frac{D\phi}{Dt} + \frac{1}{2}|\mathbf{u}|^2 - \sum_{i=1}^{q} \frac{D\mu^i}{Dt} \lambda^i \right). \tag{4}$$

B. Equations of motion for the potentials

Consider the incompressible with constant (unit) density Euler equations with a forcing term added to the right-hand side (RHS),

$$\frac{D\mathbf{u}}{Dt} = -\nabla p + \mathbf{f}[\mathbf{u}, \mathbf{x}, t], \tag{5}$$

$$\nabla \cdot \mathbf{u} = 0. \tag{6}$$

We will be concerned here with the Navier-Stokes case, where the forcing term reads

$$\mathbf{f} = \nu \Delta \mathbf{u}. \tag{7}$$

The Navier-Stokes system (5)–(7) can be used to derive an equivalent system of equations of motion for the Weber-Clebsch potentials (1). To wit, we use the RHS of the Euler equations with forcing term (5) to replace the left-hand side (LHS) of our general identity (4). This relation is then split into two parts: one that involves only gradients and another that involves the rest of the terms. This latter part can be written as

$$\frac{D\lambda^i}{Dt} = L^i[\lambda, \mu], \tag{8}$$

$$\frac{D\mu^i}{Dt} = M^i[\lambda, \mu], \tag{9}$$

where L^i, M^i obey the linear equation,

$$\sum_{i=1}^{q} (L^i \nabla \mu^i - M^i \nabla \lambda^i) = \mathbf{f} - \nabla G. \tag{10}$$

The gradient part reads

$$\frac{D\phi}{Dt} - p = \lambda^i M^i - G - \frac{1}{2}|\mathbf{u}|^2. \tag{11}$$

The arbitrary scalar, $G[\lambda, \mu]$, represents a gauge freedom stemming from the nonunique separation of a gradient part.

Let us remark at this point that the incompressibility condition (6) allows one to express ϕ in terms of λ^i and μ^i, as the solution of the linear equation,

$$\Delta \phi = \sum_{i=1}^{q} \nabla \cdot (\lambda^i \nabla \mu^i). \tag{12}$$

Thus, it is not needed to independently solve Eq. (11) for the field ϕ, since this equation is identically satisfied when ϕ is determined by the incompressibility condition (12).

Equation (10) above is a system of d linear equations for the $2q$ unknowns L^i, M^i. Note that when $\nu = 0$ (and thus $\mathbf{f} = 0$) a solution to (10) is readily obtained by setting $L^i = M^i = \mathbf{f} = G = 0$. In this case, Eqs. (8) and (9) are just the standard evolution equations for the Weber-Clebsch potentials of the Euler problem.[1]

Note also that in the overdetermined case $2q < d$ (e.g., $d=3$, $q=1$), Eq. (10) in general admits no solution. In this case it is not possible, in general, to reproduce a given $\delta\mathbf{u}$ from Eq. (2) in terms of $\delta\lambda^i$ and $\delta\mu^i$. Thus we consider from now on the case $2q \geqslant d$.

Considering from now on only the Navier-Stokes case (7), let us make a shift in the unknowns L^i, M^i, which allows the explicit introduction of dissipation in the evolution equations for the potentials,

$$L^i = \tilde{L}^i + \nu \Delta \lambda^i, \tag{13}$$

$$M^i = \tilde{M}^i + \nu \Delta \mu^i. \tag{14}$$

The evolution equations (8) and (9) for the potentials thus now read

$$\frac{D\lambda^i}{Dt} = \nu \Delta \lambda^i + \tilde{L}^i[\lambda, \mu], \tag{15}$$

$$\frac{D\mu^i}{Dt} = \nu \Delta \mu^i + \tilde{M}^i[\lambda, \mu], \tag{16}$$

and (10) is replaced by

$$\sum_{i=1}^{q} (\tilde{L}^i \nabla \mu^i - \tilde{M}^i \nabla \lambda^i) = \tilde{\mathbf{f}} - \nabla \tilde{G}, \tag{17}$$

where $\tilde{G}$ is an arbitrary scalar function, related to the former arbitrary function G by the relation $G = \tilde{G} - \nu \Delta \phi + \nu \lambda^i \Delta \mu^i$, and

$$\tilde{\mathbf{f}} = 2\nu \sum_{i=1}^{q} \sum_{\alpha=1}^{d} \partial_\alpha \lambda^i \partial_\alpha \nabla \mu^i. \tag{18}$$

The procedure to obtain $\tilde{L}^i, \tilde{M}^i$ now consists of solving the linear system (17) of d equations for $2q$ unknowns.

C. Moore-Penrose solution and minimum norm

In the underdetermined case $(2q > d)$ the general Moore-Penrose[5–7] approach corresponds to finding solutions to the linear system (17) supplemented by a requirement of minimum norm, namely that

$$\sum_{i=1}^{q} (\tilde{L}^i \tilde{L}^i + \tau^{-2} \tilde{M}^i \tilde{M}^i) \tag{19}$$

be the smallest possible. Note that in the basic Weber-Clebsch definition (1) the field $\mathbf{u}$ is a velocity with physical dimensions LT^{-1}. Thus, the product $\lambda\mu$ and the field ϕ must have dimensions L^2T^{-1}. It will turn out [see Eq. (27) below] that $[\mu] = L$ and consequently $[\lambda] = LT^{-1}$. Thus, because of relations (15) and (16), the parameter τ that appears in (19) has the dimension of time.

The general Moore-Penrose solution to (17), which minimizes the norm (19), is shown in Appendix A to be

given by (A6) and (A7). Inserting this solution in (15) and (16) we finally obtain the explicit form of the evolution equations

$$\frac{D\lambda^i}{Dt} = \nu\Delta\lambda^i + \nabla\mu^i \cdot \mathbb{H}^{-1} \cdot (\tilde{\mathbf{f}} - \nabla\tilde{G}), \tag{20}$$

$$\frac{D\mu^i}{Dt} = \nu\Delta\mu^i - \tau^2 \nabla\lambda^i \cdot \mathbb{H}^{-1} \cdot (\tilde{\mathbf{f}} - \nabla\tilde{G}), \tag{21}$$

where the dot product denotes matrix or vector multiplication of d-dimensional tensors, and $\mathbb{H}^{-1}$ is the inverse of the square symmetric $d\times d$ matrix $\mathbb{H}$, defined by its components,

$$\mathbb{H}_{\alpha\beta} \equiv \sum_{i=1}^{q} (\tau^2 \partial_\alpha\lambda^i \partial_\beta\lambda^i + \partial_\alpha\mu^i \partial_\beta\mu^i). \tag{22}$$

These evolution equations, together with the particular form of the choice for the arbitrary function $\tilde{G}$, which explicitly reads [see Eq. (A11)]

$$\tilde{G} = \Delta^{-1} \nabla \cdot \tilde{\mathbf{f}}, \tag{23}$$

represents our new algorithm.

D. Ohkitani-Constantin approach

The OC[3] approach can be directly recovered from our evolution equations (15) and (16) by supplementing the linear system (17) with the following conditions: (i) $q=d$ (thus we have d equations for $2d$ unknowns), (ii) the d extra conditions $\tilde{M}^i=0$, and (iii) $\tilde{G}=0$. When these conditions are imposed, the evolution equations for the potentials read

$$\frac{D\lambda^i}{Dt} = \nu\Delta\lambda^i + \tilde{L}^i[\lambda,\mu], \tag{24}$$

$$\frac{D\mu^i}{Dt} = \nu\Delta\mu^i, \tag{25}$$

where $\tilde{L}^i$ satisfies Eq. (17), which is now the (determined) $d\times d$ system,

$$\sum_{i=1}^{d} \tilde{L}^i \nabla\mu^i = 2\nu \sum_{i=1}^{d} \sum_{\alpha=1}^{d} \partial_\alpha\lambda^i \partial_\alpha \nabla\mu^i. \tag{26}$$

Note that the "internal" index i and the spatial index α are treated on the same footing in Eq. (26), which is only possible when $q=d$. The correspondence with the OC formulation is obtained via the change of notation $\lambda^i \to v^i$ and $\mu^i \to A^i$, respectively called "virtual velocity" and "diffusive Lagrangian map" in Ref. 3. It is straightforward to check that our Eqs. (1) and (12) are equivalent to Eqs. (3) and (4) of Ref. 3, and that our Eqs. (24) and (25) are identical to Eqs. (5) and (6) of Ref. 3.

E. Discussion

Let us return to our generalized equations (20)–(22). When $q=d$, the matrix $\mathbb{H}$ has a very simple structure in the limit $\tau\to 0$ [see Eq. (22)]. Indeed it can be written (with obvious notation) as $\mathbb{H}=(\nabla\boldsymbol{\mu})\cdot(\nabla\boldsymbol{\mu})^T$. It is thus straightforward to show that our new algorithm (20) and (21) (with the particular gauge choice $\tilde{G}=0$) reduces in the limit $\tau\to 0$ to the Ohkitani-Constantin approach (24)–(26). Note that the existence of a solution to (26) requires (in general) that the matrix $(\nabla\boldsymbol{\mu})$ be invertible. Problems will thus generically occur when $\det(\nabla\boldsymbol{\mu})=0$, which is on a manifold of codimension 1. Thus, for any space dimension d, the generic situation is that for every point of space $(x^1,\ldots,x^d)$ there exists a time t^* at which the determinant becomes zero.

However, if we do not take the particular choice $\tilde{M}^i=0$, then the solution of the linear system (17) of d equations for $2d$ unknowns generically will be ill defined in a manifold of codimension $(d+1)$, i.e., on isolated points in space time. The corresponding Moore-Penrose solution to (17) requires the invertibility of the matrix $\mathbb{H}=(\nabla\boldsymbol{\mu})\cdot(\nabla\boldsymbol{\mu})^T + \tau^2(\nabla\boldsymbol{\lambda})\cdot(\nabla\boldsymbol{\lambda})^T$.

Thus, because the condition $\det(\nabla\boldsymbol{\mu})=0$ is generically obtained at lower codimension than the condition $\det\mathbb{H}=0$, the limit $\tau\to 0$ is *singular*.

III. NUMERICAL RESULTS

A. Implementation

Spatially periodic velocity fields can be generated from the Weber-Clebsch representation (1) by setting

$$\mu^i = x^i + \mu_p^i, \tag{27}$$

and assuming that μ_p^i and the other fields λ^i and ϕ appearing in (1) are periodic. Indeed, any given periodic velocity field $\mathbf{u}$ can be represented in this way by setting

$$\mu_p^i = 0, \tag{28}$$

$$\lambda^i = u^i, \tag{29}$$

$$\phi = 0. \tag{30}$$

Note that the time-independent nonperiodic part of μ^i of the form given in (27) is such that the *gradients* of μ^i are periodic. It is easy to check that this representation is consistent with the generalized equations of motions (20) and (21).

Our numerical study will be performed using the so-called Taylor-Green[4] single-mode initial condition,

$$u^1 = \sin x \cos y \cos z,$$

$$u^2 = -\cos x \sin y \cos z, \tag{31}$$

$$u^3 = 0.$$

As the initial length and velocity scales are of order 1, the Reynolds number will be defined by $R=1/\nu$ (Ref. 8).

Standard Fourier pseudospectral methods are used both for their precision and for their ease of implementation.[9] Symmetries are employed to reduce memory storage and speed up computations. The runs presented below were performed at resolution 192^3. Implementation details are given in Appendix B.

In what follows, we will systematically compare the velocity field $\mathbf{u}$, obtained from (1) and (12) by evolving the

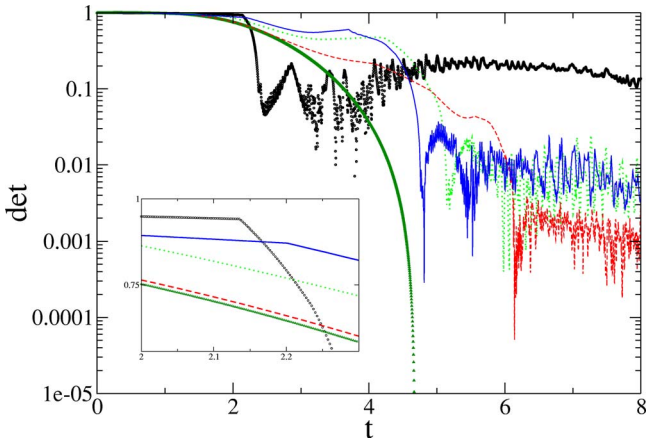

FIG. 1. (Color online) Time evolution of the minimum of det($\mathbb{H}$) [see Eq. (22)] at Reynolds number $R=40$ with $\tau=0$, 0.01, 0.1, 0.2, and 1 (from bottom to top at $t=2.1$, see inset).

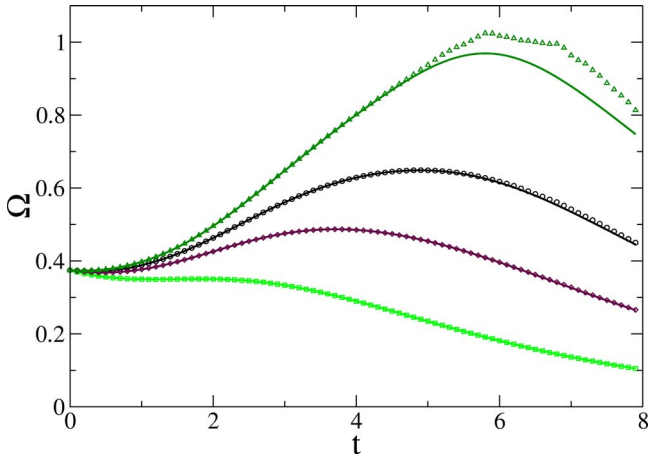

FIG. 2. (Color online) Time evolution of enstrophy Ω at Reynolds numbers $R=40$, 70, 100, and 150 (□, ◇, ○, and △), and $\tau=1$. Straight lines are DNS of Navier-Stokes equations.

Weber-Clebsch potentials using (20), (21), and (23), with the velocity field obtained by direct Navier-Stokes evolution from the Taylor-Green initial data (31).

B. Integration without resetting

Let us first consider computations performed *without* resetting. Equations (28)–(30) are thus used only once, to initialize the Weber-Clebsch potentials at the start of the calculation.

The time evolution of the spatial minimum of the determinant of the matrix $\mathbb{H}$, defined in Eq. (22), is displayed in Fig. 1 for various values of τ. It is manifest in the figure that, in the OC limit, when $\tau=0$, the minimum of the determinant reaches zero after a finite time. Then, the computation *cannot* be continued. However, when $\tau\neq 0$, the determinant stays positive and the computation *can* be carried on. This behavior of the determinant is consistent with the issues about the invertibility of $\mathbb{H}$ that were discussed above in Sec. II E. The singular nature of the $\tau\to 0$ limit is therefore discernible in the figure.

In order to characterize the precision of the $\tau\neq 0$ Weber-Clebsch algorithm we now compare its results with direct Navier-Stokes calculations. More precisely, we compare the associated enstrophy $\Omega(t)=\Sigma_k k^2 E(k,t)$ and energy spectrum $E(k,t)$, where the energy spectrum is defined by averaging the Fourier transform $\hat{\mathbf{u}}(\mathbf{k}',\mathbf{t})$ of the velocity field (1) on spherical shells of width $\Delta k=1$,

$$E(k,t)=\frac{1}{2}\sum_{k-\Delta k/2<|\mathbf{k}'|<k+\Delta k/2}|\hat{\mathbf{u}}(\mathbf{k}',\mathbf{t})|^2. \tag{32}$$

It is apparent in Fig. 2 that the enstrophy computed at resolution 192^3 is well resolved, provided that the Reynolds number stays well below $R\simeq 150$. Thus, for $\tau=1$, our generalized algorithm (20) and (21) reproduces well the Navier-Stokes dynamics *for all times*, provided that the Reynolds number is not too large. This suggests that, in order to trace the Navier-Stokes dynamics without resetting, τ could be matched depending on Reynolds number. This possibility will be studied in future work. We have checked (data not shown) that the limiting Reynolds number is an increasing function of resolution.

Time evolution of the energy spectrum is presented in Fig. 3. It is conspicuous in the figure that an error is present at large wavenumber, even when the vorticity is very well resolved (compare with the lowest Reynolds number in Fig. 2). When time increases from 1 to 2.5 (the time at which the determinant reaches its first minimum, see the $\tau=1$ curve in Fig. 1), the wavenumber above which an error is visible decreases and the level of the error increases. However, for later time this trend is visibly reversed: the error has actually *decreased* at $t=7.5$.

C. Integration with resettings

Following Ohkitani and Constantin,[3] we now turn our attention to computations performed *with* resettings. Equations (28)–(30) are thus used not only to initialize the Weber-

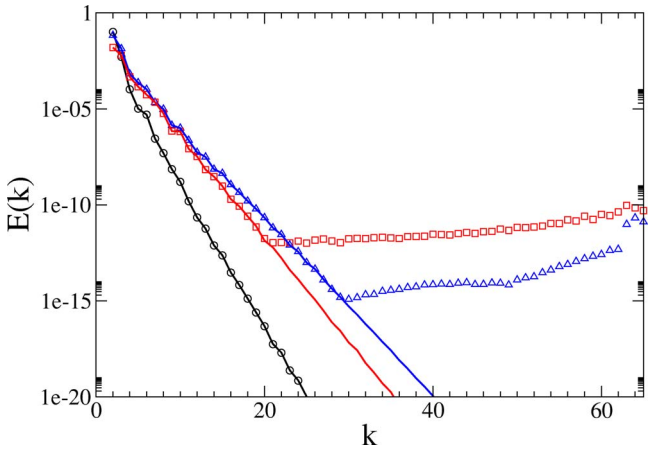

FIG. 3. (Color online) Evolution of the energy spectrum at Reynolds number $R=40$ for $t=1$, 2.5, and 7.5 (○, □, and △), and $\tau=1$. Straight lines are DNS of Navier-Stokes equations.

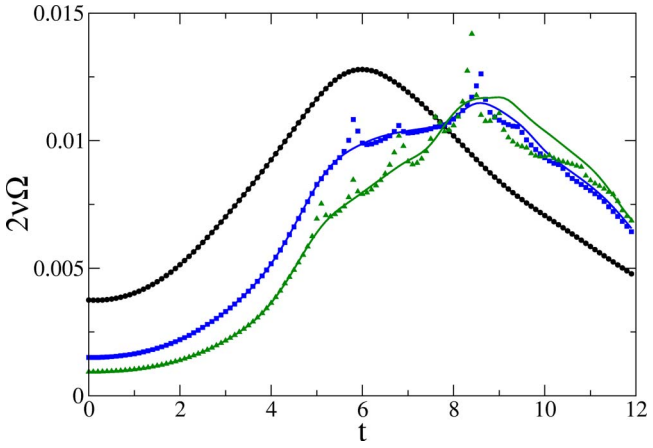

FIG. 4. (Color online) Time evolution of $2\nu\Omega$ with $\tau=1$ and resetting threshold $\epsilon^2=0.01$ at Reynolds numbers $R=200$, 500, and 800 (○, □, and △). Straight lines are DNS of Navier-Stokes equations.

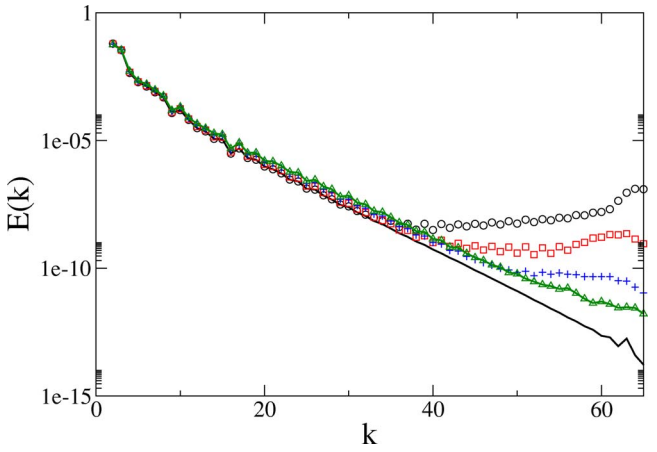

FIG. 5. (Color online) Time evolution of energy spectrum after resetting at Reynolds number $R=200$ with $\tau=0.01$, at $t=3.6$ (just after resetting), 3.7, 3.8, and 3.9 (○, □, +, and △) Straight lines are DNS of Navier-Stokes equations at $t=3.6$ and 3.9.

Clebsch potentials at the start of the calculation but also to *reset* them to the current value of the velocity **u**, obtained from (1) and (12), whenever the minimum of the determinant of the matrix (22) falls below a given threshold,

$$\det(\mathbb{H}) \leqslant \epsilon^2. \tag{33}$$

Note that this definition agrees with the resetting criterion of OC[3], $|\det(\nabla\boldsymbol{\mu})| \leqslant \epsilon$ because, in the limit $\tau \to 0$, $\det(\mathbb{H}) = \det(\nabla\boldsymbol{\mu})^2$ (see Sec. II E above). Ohkitani and Constantin have related the vanishing of $\det(\nabla\boldsymbol{\mu})$ to unusually intense particle diffusion that takes place near reconnection. In the generalized formalism, the fields $(\boldsymbol{\lambda}(\mathbf{x},t),\boldsymbol{\mu}(\mathbf{x},t))$ are treated essentially on the same footing; thus, it is expected that the phenomenon of intense particle diffusion will be associated with the degeneracy of an object that involves both of them. It is tempting to speculate that this object is $\det(\mathbb{H})$. This matter will be studied in the future.

It is clear in Fig. 4 that the enstrophy computed at resolution 192^3, using resetting with threshold $\epsilon^2=0.01$ and $\tau=1$, is well resolved, provided that the Reynolds number stays below $R \simeq 800$. Figure 4 thus shows that performing resettings allows computation at much higher Reynolds numbers than without resetting (compare with Fig. 2).

A simple dynamical mechanism for the decrease of the determinant $\det(\mathbb{H})$ is the effect of the advection term in Eqs. (15) and (16) that tends to align all the gradients $\nabla\boldsymbol{\lambda}$ and $\nabla\boldsymbol{\mu}$ with the same strain eigendirection (data not shown). This behavior leads to a loss of numerical precision in the solution of the linear system (17) or, equivalently, in the invertibility of the matrix $\mathbb{H}$ [Eq. (22)]. Note that this behavior is cured when performing a resetting.

The time evolution of the error on the energy spectrum is displayed in Fig. 5. It is visible in the figure that, following a resetting, the errors present at high wavenumbers decay rapidly. This shows that right after a resetting Navier-Stokes dynamics is restored at the smallest scales, thereby allowing "auto healing" of the spectrum.

The influence of the parameter τ on the errors is shown in Fig. 6. It is apparent in the figure that the errors prior to resetting are larger for $\tau=0.1$ than when $\tau=0$. However, note that the errors at the end of the run are small and of the same order of magnitude in both cases (see also Fig. 4).

D. Frequency of resetting

The influence of the parameter τ on the temporal distribution of the intervals $\Delta t_j = t_j - t_{j-1}$ between resetting times t_j, at fixed value of the resetting threshold $\epsilon^2=0.01$, is displayed in Fig. 7. It can be seen in the figure that, at a given time, the interval is (generally) an increasing function of τ, but that the prevailing behavior in time of Δt is well preserved when τ is small enough. Note that, for $t \simeq 10$, the intervals Δt between resettings are observed to increase from $\Delta t \simeq 0.25$ to $\Delta t \simeq 0.5$ when τ is varied from 0 to 0.01. More information on the influence of small nonzero τ on the resetting frequency is obtained by looking at the total number of resettings, between $t=0$ and $t=12$ presented in Table I. The table shows that the total number of resettings decreases when τ is increased from 0 to 0.001. Note that this effect takes place for values of τ much smaller than Δt.

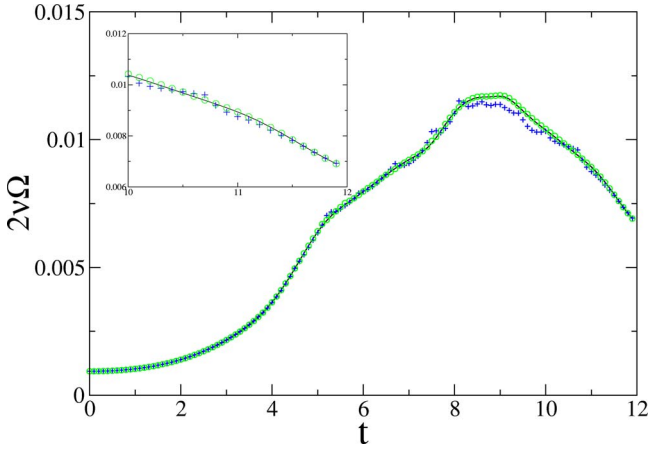

FIG. 6. (Color online) Time evolution for $2\nu\Omega$ at Reynolds number $R=800$ for $\tau=0$ and 0.1 (○ and +). The straight line is a DNS of Navier-Stokes equations.

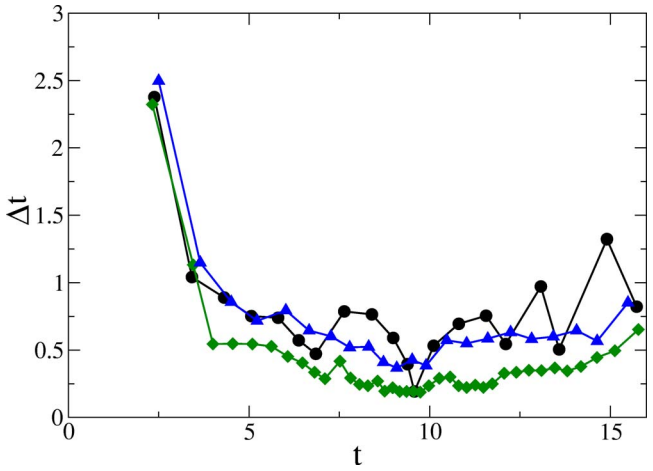

FIG. 7. (Color online) Time evolution of the intervals between resettings Δt_j vs resetting time t_j at Reynolds number $R=800$ for $\tau=0$, 0.01 and 1 ($\diamond$, $\triangle$ and $\bigcirc$).

IV. CONCLUSION

A. Summary

We derived generalized equations of motion for the Weber-Clebsch potentials that imply that the velocity field follows Navier-Stokes equations. These new equations were shown to depend on τ (a parameter with the dimension of time) and to reduce to the OC equations in the singular limit $\tau \to 0$. DNS of the viscous Taylor-Green vortex were performed and the influence of the parameter τ was characterized. For $\tau \neq 0$, it was possible to perform computation *without* resetting and the Navier-Stokes dynamics was well reproduced for small enough Reynolds numbers. However, errors were found to be present at large wavenumbers, even when the vorticity was well resolved. Performing resettings allowed us to compute at much higher Reynolds numbers and the level of error was found to rapidly decay following each resetting. The intervals Δt between resettings were found to sharply increase when τ was varied from 0 to a value much smaller than Δt.

B. Discussion

The present numerical study was performed on the Taylor-Green vortex, a flow in which vorticity layers are formed in the early stage, followed by their rolling up by Kelvin-Helmholtz instability.[8] In contrast, Ohkitani and Constantin[3] chose a flow that initially consists of two orthogonally placed vortex tubes. This flow was previously used by Boratav, Pelz, and Zabusky (BPZ)[10] to study in detail vortex reconnection. It can be argued[3] that cut-and-connect-type reconnections are much more pronounced in the BPZ flow than in the Taylor-Green flow. Indeed, when comparing the present Fig. 7 with Fig. 3 of OC, it is apparent that the minimum of Δt is much more pronounced in the BPZ flow than in the Taylor-Green flow. Detailed comparison, performed on the BPZ flow, of Δt computed at $\tau \neq 0$ with the Δt of OC, will be reported in the future. Extensions of the present approach to compressible and magnetohydrodynamics flows will also be reported elsewhere.

TABLE I. Variations with τ of the total number of resettings between $t=0$ and $t=12$ (same conditions as in Fig. 7).

Value of τ	Number of resettings
0.0	29
0.001	20
0.005	17
0.01	16
0.05	14
0.1	15
1.0	13

ACKNOWLEDGMENTS

We acknowledge very useful scientific discussions with Peter Constantin and Edriss S. Titi. One of the authors (M.E.B.) acknowledges support from an ECOS/CONICYT action.

APPENDIX A: MOORE-PENROSE SOLUTION

1. Minimizing the local norm

Following the general Moore-Penrose[5–7] approach, we seek solutions to the linear system (17) supplemented by the requirement that the norm (19) be the smallest possible at each point in space and time. These solutions can be directly obtained by minimizing the following function with respect to all of its arguments:

$$\mathcal{S}(\tilde{L}^i,\tilde{M}^i,\mathbf{k}) = \tfrac{1}{2}\sum_{i=1}^{q} (\tilde{L}^i\tilde{L}^i + \tau^{-2}\tilde{M}^i\tilde{M}^i) - \mathbf{k}\cdot\left(\sum_{i=1}^{q} (\tilde{L}^i \nabla \mu^i - \tilde{M}^i \nabla \lambda^i) - \tilde{\mathbf{f}} + \nabla\tilde{G}\right). \tag{A1}$$

Indeed, the equations $\partial\mathcal{S}/\partial k=0$ correspond to the original system (17) and, when this system is satisfied, the equations $\partial\mathcal{S}/\partial\tilde{L}^i=0$ and $\partial\mathcal{S}/\partial\tilde{M}^i=0$ imply that the norm is minimal. These equations explicitly give the unknowns in terms of the Lagrange multiplier $\mathbf{k}$,

$$\tilde{L}^i = \mathbf{k}\cdot\nabla\mu^i, \tag{A2}$$

$$\tilde{M}^i = -\tau^2\mathbf{k}\cdot\nabla\lambda^i. \tag{A3}$$

Inserting these solutions into (17) yields the following equation for the Lagrange multiplier:

$$\mathbb{H}\cdot\mathbf{k} = \tilde{\mathbf{f}} - \nabla\tilde{G}, \tag{A4}$$

where the square symmetric $d\times d$ matrix $\mathbb{H}$ is defined by its components

$$\mathbb{H}_{\alpha\beta} \equiv \sum_{i=1}^{q} (\tau^2\partial_\alpha\lambda^i\partial_\beta\lambda^i + \partial_\alpha\mu^i\partial_\beta\mu^i). \tag{A5}$$

When $\mathbb{H}$ is invertible, the solution for the unknowns explicitly reads

$$\tilde{L}^i = \nabla\mu^i \cdot \mathbb{H}^{-1} \cdot (\tilde{\mathbf{f}} - \nabla\tilde{G}), \tag{A6}$$

$$\tilde{M}^i = -\tau^2 \nabla\lambda^i \cdot \mathbb{H}^{-1} \cdot (\tilde{\mathbf{f}} - \nabla\tilde{G}). \tag{A7}$$

Finally, we define the Moore-Penrose norm, which is the norm $\mathcal{S}(\tilde{L}^i, \tilde{M}^i, \mathbf{k})$ in Eq. (A1) evaluated on the above solution. We get

$$\mathcal{S}_{\mathrm{MP}}[\tilde{G}] = \tfrac{1}{2}(\tilde{\mathbf{f}} - \nabla\tilde{G}) \cdot \mathbb{H}^{-1} \cdot (\tilde{\mathbf{f}} - \nabla\tilde{G}). \tag{A8}$$

2. Minimizing the space integral of the Moore-Penrose norm using $\tilde{G}$

Notice that the function $\tilde{G}$ remains arbitrary. Given the function $\tilde{G}$ there is a solution given by (A6) and (A7), which minimizes the norm to the value given by Eq. (A8). We determine $\tilde{G}$ by the further requirement of minimum value of the integral throughout space of the norm $\mathcal{S}_{\mathrm{MP}}[\tilde{G}]$ multiplied by a given weight function $W(x^\alpha)$,

$$S[\tilde{G}] = \tfrac{1}{2}\int_\Omega (\tilde{\mathbf{f}} - \nabla\tilde{G}) \cdot \mathbb{H}^{-1} \cdot (\tilde{\mathbf{f}} - \nabla\tilde{G}) W(x^\alpha) d^d x. \tag{A9}$$

Variation with respect to $\tilde{G}$ gives the Euler-Lagrange equation,

$$\nabla \cdot (W\mathbb{H}^{-1} \cdot (\tilde{\mathbf{f}} - \nabla\tilde{G})) = 0, \tag{A10}$$

which is an inhomogeneous, linear, second-order partial differential equation for $\tilde{G}$.

In practice we solve the simpler equation,

$$\nabla \cdot (\tilde{\mathbf{f}} - \nabla\tilde{G}) = 0. \tag{A11}$$

Note that this equation is straightforward to solve and is strictly equivalent to (A10) only for constant $\mathbb{H}$. However, we find that in the general case of nonconstant $\mathbb{H}$ this simple choice leads to a stable algorithm.

APPENDIX B: NUMERICAL METHODS

Symmetries of the Weber-Clebsch representation are employed to reduce memory storage and speed up computations. Our numerical methods are thus standard; their only specialty stems from the conjunction of the Taylor-Green symmetries with the Weber-Clebsch representation (1).

1. Symmetric Weber-Clebsch representation

The symmetries of the Taylor-Green velocity field (31) implemented in the code are rotational symmetry of angle π around the axis $(x=z=\pi/2)$, $(y=z=\pi/2)$, and $(x=y=\pi/2)$, and mirror symmetry with respect to the planes $x=0,\pi$, $y=0,\pi$, $z=0,\pi$. These planes form the sides of the so-called *impermeable box*, which confines the flow. These symmetries correspond to the following particular form for the nonzero Fourier modes of the velocity field solution of the Navier-Stokes equations:

$$\begin{aligned} \hat{u}^1(m,n,p,t) &\quad \sin mx \cos ny \cos pz, \\ \hat{u}^2(m,n,p,t) &\quad \cos mx \sin ny \cos pz, \\ \hat{u}^3(m,n,p,t) &\quad \cos mx \cos ny \sin pz, \end{aligned} \tag{B1}$$

where $\hat{\mathbf{u}}(m,n,p,t)$ vanishes unless m,n,p are either all even or all odd integers. Separation of the even and odd parts and the use of special sine/cosine Fourier transforms reduces memory storage and speeds up computations.[8]

It is easy to directly check from the Weber-Clebsch representation (1) and (27) that the fields λ^i and μ_P^i admit exactly the same representation (B1) than the velocity field u^i, while the field ϕ admits the similar representation that only involves cosines.

2. Moore-Penrose implementation

In order to save memory and operation count, the right-hand side of (18) is evaluated as

$$\nu\sum_{i=1}^{q} (\Delta u - \Delta\lambda^i \nabla\mu^i - \lambda^i \Delta\nabla\mu^i - \Delta\nabla\phi). \tag{B2}$$

This expression yields a result identical to (18), because we perform dealiasing using the 2/3 rule.[9] In a computation cycle, Eq. (23) is first used to obtain $\tilde{G}$ in spectral space. The velocity field obtained from (1) and (12) is dealiased by the 2/3 rule. The matrix elements (22) and the full nonlinear terms of (20) and (21) are then computed in physical space. The nonlinear terms are dealiased in spectral space. Adams-Bashforth time stepping is used to update the potentials. Due to dealiasing, computations performed at resolution N (with N grid points between 0 and 2π) have a maximum wavenumber $k_{\max}=N/3$.

[1] H. Lamb, *Hydrodynamics* (Cambridge University Press, Cambridge, UK, 1932).
[2] P. Constantin, "An Eulerian-Lagrangian approach to the Navier-Stokes equations." Commun. Math. Phys. **216**, 663 (2001).
[3] K. Ohkitani and P. Constantin, "Numerical study of the Eulerian-Lagrangian formulation of the Navier-Stokes equations." Phys. Fluids **15**, 3251 (2003).
[4] G. I. Taylor and A. E. Green, "Mechanism of the production of small eddies from large ones." Proc. R. Soc. London, Ser. A **158**, 499 (1937).
[5] E. H. Moore, "On the reciprocal of the general algebraic matrix." Bull. Am. Math. Soc. **26**, 394 (1920).
[6] R. Penrose, "A generalized inverse for matrices." Proc. Cambridge Philos. Soc. **51**, 406 (1955).
[7] A. Ben-Israel and T. N. E. Greville, *Generalized Inverses: Theory and Applications* (Wiley-Interscience, New York, 1974).
[8] M. E. Brachet, D. I. Meiron, S. A. Orszag, B. G. Nickel, R. H. Morf, and U. Frisch, "Small-scale structure of the Taylor-Green vortex." J. Fluid Mech. **130**, 411 (1983).
[9] D. Gottlieb and S. A. Orszag, *Numerical Analysis of Spectral Methods* (SIAM, Philadelphia, 1977).
[10] O. N. Boratav, R. B. Pelz, and N. J. Zabusky, "Reconnection in orthogonally interacting vortex tubes: Direct numerical simulations and quantifications." Phys. Fluids A **4**, 581 (1992).